Reaction Kinetics, Mechanisms and Catalysis (2024) 137:2147–2171
https://doi.org/10.1007/s11144-024-02644-8

Heterogeneity of adsorption and reaction sites on the surface of (10%Co + 0.5%Pd)/TiO_2 catalysts during CO hydrogenation

Maya Shopska[1] · Krassimir Tenchev[1] · Georgi Kadinov[1] · Hristo Kolev[1] · Martin Fabian[2] · Katerina Aleksieva[1]

Received: 11 March 2024 / Accepted: 30 April 2024 / Published online: 23 May 2024

Abstract

Adsorption and reaction site heterogeneity of titania-supported (10%Co + 0.5%Pd) catalysts in CO hydrogenation was studied by chemisorption, temperature-programmed desorption, and diffuse reflectance infrared Fourier transform spectroscopy techniques. Precursor material was treated in various media as reductive, inert, or oxidative. Cobalt metal sites and TiO_2 support heterogeneity were proved. Upon H_2 chemisorption, a pre-reduced sample exposed mostly homogeneous metal surface. Surface heterogeneity toward CO chemisorption depended on preliminary treatment. A catalyst prepared in inert medium revealed moderate activity dynamics of adsorption and reaction sites. Weak to medium strength sites toward hydrogen adsorption were relatively strong in terms of CO adsorption. Carbonate-(like) species occupied medium and strong sites on the support. Sites of weak strength for CO adsorption were active in hydrogenation but very strong in terms of CH_x intermediates adsorption.

Graphical abstract

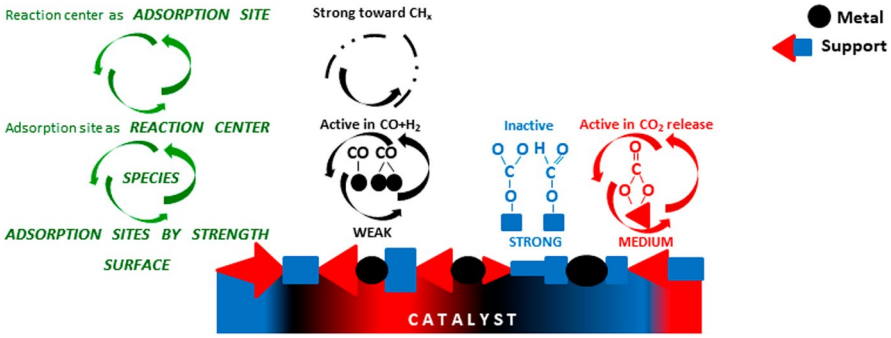

Extended author information available on the last page of the article

Keywords CO hydrogenation · Bimetallic Co–Pd catalysts · Titania support · Adsorption and reaction sites · Surface heterogeneity · In situ infrared spectroscopy

Introduction

CO hydrogenation to hydrocarbons is a process which is exploited for years in succession. In broad terms the process is described as kind of polymerization. The monomer is formed at catalyst surface and then it is imported into increasing C–C chain. Existence of more than one monomer is possible. There are different suppositions about the process mechanism but without unanimous opinion [1]. The CO insertion mechanism (hydroformylation) is based on CO insertion into Me–H or Me–R followed by sequential hydrogenation and elimination of water. The enol mechanism supposes that condensation of adjacent Me=CHOH occurs and is followed by elimination of water. The carbide (carbene) mechanism says that CO dissociates on the surface to surface carbide and then it is sequentially hydrogenated to CH, CH_2, CH_3 and CH_4 or higher hydrocarbons. In this mechanism CH or CH_2 are considered as the chain initiators and propagators [1, 2]. Both cobalt and palladium metals are active alone in the reaction to promote synthesis of different compounds from the same reagents [3–5]. Palladium-promoted cobalt catalysts are widely studied too for CO hydrogenation [6–15]. Adsorption of reagents, intermediates, and products is an important step in the reaction mechanism of heterogeneous catalytic processes. The catalyst itself and existence of stable adsorbates and spectator species can impede identification of the real intermediates. Studying carbon monoxide hydrogenation, the CO molecule operates in the reaction as both a reagent and a probe, which provides information about the catalyst surface.

Adsorption sites are examined by type, strength, and quantity. Hydrogen chemisorption, being dissociative, determines only Co^0 and Pd^0 sites and is usually regarded as linear (atop) type of Me–H configuration. Hydrogen temperature-programmed desorption (TPD) is used to distinguish sites by strength due to the peak position whereas the peak area allows determination of site relative amount. Hydrogen adsorption cannot be revealed by infrared spectroscopy (IRS) itself, however it provides indirect strategy to obtain relevant conclusions [16]. CO adsorbs on Co^0 and Co^{n+}, Pd^0 and Pd^{n+}, and support. Adsorption can be linear or multicenter as well as associative and dissociative. TPD of CO gives information about site strength and, in combination with IRS study, is helpful to determine the type of adsorbed species.

Factors and aspects of the (metal) particle surface heterogeneity.

Throughout reaction, the adsorption sites may work like reaction sites as well due to appropriate properties like energy, strength, and stability [17]. Different factors may affect the functions, which an adsorption site performs in reaction: reduction, reconstruction, agglomeration, electronic effect, structural (ensemble) effect, etc. [18, 19]. Certain adsorption sites might be low active or inactive in a studied reaction but

could be activated under reaction conditions. Below effect of several factors and aspects of their influence on the surface sites heterogeneity are discussed.

Reduction and heterogeneity

Reduction of cobalt oxide phases is a stage in the preparation of catalysts with application in CO hydrogenation. It has been found that well reduced cobalt sites bind more strongly carbon monoxide [20]. Together with Co^0 sites, using CO adsorption, are also registered Co^{2+} and $Co^{\delta+}$ sites on the catalysts as well as sites designated as α, γ, δ, β distinguished by the strength of interaction with the support [20–22]. During high temperature adsorption (230–300 °C) of CO on surface with preadsorbed hydrogen it has been established larger amount of adsorbate, new adsorption sites disclosure in comparison with the same experiment but carried out at room temperature [23]. A different infrared band is registered when CO and H_2 are co-adsorbed compared to sole adsorption of CO and it is denoted as characteristic about H–Co–CO species [24].

Reconstruction and heterogeneity

CO adsorption can give rise to linearly and multi-bonded species. The couples of bands at 1937/2035 and 1974/2054 cm^{-1} represent couples of CO adsorbed linear and bridge and are assigned, respectively, to adsorption on hexagonal and cubic cobalt [24]. There is a possibility for transforming surface species due to site reconstruction and adsorbate amount under reaction conditions. The catalyst surface contains different crystal facets. During adsorption and reaction the type of the facets and ratio between them can change continuously because the atoms building them up participate in the processes [25]. Thus, part of the surface may operate only as adsorption sites and another fraction may act as reaction sites [26, 27]. In turn, the latter sites, depending on their structure, participate with varying probability in hydrocarbon chain growth and/or hydrogenation reactions [28, 29]. It is established that the preferred mechanism of carbon chain lengthening over hexagonal Co is affected by type of the exposed facet. There are reports about studies on Co(10–10), Co(10–11), and Co(0001) facets. So for example preferred facet and mechanism of C–C chain increase are, respectively, Co(10–10) and carbide mechanism than Co(0001) and CO insertion mechanism [30, 31].

Electron and ensemble effect and heterogeneity

Palladium and cobalt form bulk mixed phases [6–8, 32–34] that determine versatility of surface composition and development of adsorption sites with modified properties. A combination of metal atoms on the surface of bimetallic particles results in a decrease of the number of sites responsible for multicenter CO adsorption [18, 35] and diminished stability of the surface species [36]. Using a carrier with catalytically active phase brings in additional element of heterogeneity having three aspects of behavior as a new constituent that induces new features in the system. The support is characterized by own heterogeneity determined

from crystal structure and changes induced in carrier electronic structure at the boundary with a supported metal particle and/or in its vicinity [9, 37–41]. Porosity of carrier can affect adsorption properties too as in case of large pores large well reduced metal crystallites can be formed [24]. Intrinsic to titania is the phenomenon of strong metal-support interaction (SMSI) that may appear at different stages of catalyst formation and work [42–47]. Titania special features may lead to changes in cobalt dispersion. Possibility for alloy formation and changes in carrier before and during reaction may create additional adsorption and reaction sites as well as modification of existing traditional centers.

Also opinion about site function has been suggested that linear adsorption, dissociation and CO insertion are accomplished at same active site. Other type of site, for direct dissociation, is linked to high hydrogenating activity but quick deactivation [20]. Adsorption site, being inactive in CO dissociation or hydrogenation, may participate in hydrogen activation, i.e. to serve as reaction site for H_2 dissociation under reaction conditions.

In respect to the discussed above evidence, this work considers adsorption and reaction site heterogeneity of TiO_2-supported (10%Co + 0.5%Pd) catalysts in the reaction of CO hydrogenation.

Experimental

Materials

$Co(NO_3)_2 \cdot 6H_2O$ and $Pd(NO_3)_2 \cdot 2H_2O$ were used for synthesis of catalysts. The salts were of pro analysi quality Merck products. Non-porous TiO_2 carrier P25 type with specific surface 50 m^2/g was commercial product of Degussa. The purity of gases applied in different stages of the investigation was 5.0 grade except for carbon monoxide that was of 3.5 grade. Unless another provider is indicated, Messer Bulgaria, part of the Messer Group, supplied all gases and gas mixtures used in this study.

Synthesis and pretreatment of catalyst material

Bimetallic (10%Co and 0.5%Pd) catalyst precursor was prepared by deposition of metal nitrate salts from aqueous solution on TiO_2. Previous investigations have shown the selected composition of the studied system to be optimal [10, 11, 48]. Obtained suspension was dried at 60 °C in vacuum for 24 h. Portions of dried precursor were treated solely in a flow of either hydrogen or Ar, or air in a procedure of successive heating at 100, 200, and 300 °C for 1 h at a heating rate of 100 °C/h between steps. This pretreatment mode was carried out in situ in the measuring cell of applied device. According to used medium (H_2, air, Ar/N_2) thus prepared catalyst samples were denoted as (red), (ox), and (inert) after precursor treatment.

Characterization technics and related calculations

Quantities of the chemical elements in the prepared catalyst material were determined using an inductively coupled plasma atomic emission spectrometer (ICP-AES) model 3410 with a mini burner and a vacuum system (ARL, USA). Measurements were carried out after acid decomposition of the solid substance.

Chemisorption of hydrogen and carbon monoxide (Fluka) was measured on reduced catalyst samples by volumetric method in an all glass device using 150 mg of the substance. H_2 (CO) adsorption determined by this method is not selective toward cobalt and palladium, i.e. a fraction of both metals on the sample surface could not be distinguished. Monolayer capacity a_{mono} was calculated after successive reduction at 300 and 400 °C for 1 h and at 450 °C for 2 h in hydrogen flow followed by evacuation to $P = 1 \times 10^{-5}$ Torr at 450 °C. Experimental determination was realized by back extrapolation of the linear isotherm saturation branch to zero pressure. Hydrogen adsorption isotherms were obtained at a temperature of 100 °C in order to minimize absorption in the bulk of palladium [49] and to activate adsorption on cobalt [50, 51]. CO chemisorption was measured at room temperature. The fraction of irreversibly (strongly) adsorbed CO was calculated as difference between the total and reversible (weak) chemisorption. Experimentally, this was accomplished by measuring the total CO adsorption, evacuation at room temperature to 10^{-6} Torr, and measuring the reversible CO adsorption [42]. Irreversible adsorption of CO further in the text will be referred simply as "CO adsorption". Dispersion of the catalytically active metal was calculated from hydrogen chemisorption data by the following formula: $D_H = N_s/N = a_{mono} \cdot X \cdot A_{Co} \cdot A_{Pd}/(C_{Co} \cdot A_{Pd} + C_{Pd} \cdot A_{Co})$, where N_s is the number of metal atoms on the surface, N is the total number of metal atoms in the sample, a_{mono} is monolayer capacity (mol/g), X is stoichiometry of adsorption (in the case of hydrogen $X = 2$), A_{Co} and A_{Pd} are respective element atomic masses (g/mol), and C_{Co} and C_{Pd} are element contents in the catalyst expressed as parts of the unit (1).

In order to study adsorption–desorption equilibrium experimental data was adjusted to the models of Freundlich and Langmuir [42, 52–54]. The equation $a = a_{mono} \cdot K_L \cdot p/(1 + K_L \cdot p)$ represents Langmuir model of adsorption isotherm [52, 54, 55]. The meaning of the parameters is as follows: a—equilibrium adsorbed amount (μmol/g), a_{mono}—adsorption capacity of monolayer (μmol/g), p—equilibrium adsorbate pressure (Torr) and K_L—Langmuir constant ($Torr^{-1}$). K_L is inversely proportional to enthalpy of adsorption, ΔH_{ads}, and activation energy. The equation $a = K_F \cdot p^{1/n}$ represents Freundlich isotherm [52, 54, 56]. Isotherm parameters are: a—adsorbed amount at equilibrium (μmol/g), p—equilibrium pressure (Torr), K_F—relative adsorption capacity ($\mu mol/g.Torr^{1/n}$). Factor n accepts values between 0 and 10 and represents adsorption deviation from linearity, i.e. it is related to heterogeneity. Values of $n < 1$ are indicative of disadvantageous adsorption/low sorption capacity. The exponent can accept values $1 \geq 1/n$ or $1 \leq 1/n$ [57, 58].

Catalyst characterization by scanning electron microscopy (SEM), transmission electron microscopy (TEM), electron paramagnetic resonance spectroscopy (EPR), photon cross-correlation spectroscopy (PCCS), and X-ray photoelectron

spectroscopy (XPS) was done using samples initially tested for catalytic activity in CO hydrogenation. The conditions used for catalytic tests and analytical methods can be found elsewhere [12, 13].

Microscopy studies were applied to inspect and visualize morphology of catalysts. A Topcon EM-002B transmission electron microscope (Japan) working with acceleration voltage of 200 keV, resolution of 1.8 Å, and possibility about 100 to 2×10^6 magnification of the real object was used. Energy dispersive X-ray analysis (EDX) of selected 14-nm diameter areas from samples was performed by KEVEC analyzer. In addition, a MIRA3 FE-SEM scanning electron microscope (TESCAN, Czech Republic) working at accelerating voltage up to 30 kV and magnification up to 10^6 was used. An EDX accessory (Oxford Instruments, UK) of the microscope allowed determination of chemical composition.

Ex situ spectra based on EPR phenomenon were recorded on a JEOL JES-FA 100 EPR spectrometer (Japan) operating in X-band with standard TE011 cylindrical resonator. An ES-DVT4 Varied Temperature Controller provided spectra detection at a temperature of − 150 °C. The desired low temperature was achieved by a cooling gas (liquid nitrogen) system, which was controlled by spectrometer computer.

PCCS was applied to determine particle size distribution in the studied materials. Data were derived by a Nanophox instrument (Sympatec GmbH, Germany). Samples were dispersed in distilled water, and then the suspensions were exposed to supersonic treatment for 15 min. The cuvette with suspension was placed in a thermo-controlled holder (25 °C) at least 5 min before measurement commencement. Five measurements of each sample were carried out for a period of 900 s.

XPS was used to study sample surface after catalytic measurements. Analysis was carried out using ESCALAB MkII (VG Scientific, UK) electron spectrometer at a base pressure in the analysis chamber of 5×10^{-10} mbar (during the measurement $1\text{x}10^{-8}$ mbar), using Al K_α X-ray source with excitation energy $h\nu = 1486.6$ eV. Pass energy of the hemispherical analyzer was 20 eV with 6-mm slit widths of entrance and exit. Instrumental resolution measured as the full width at a half maximum (FWHM) of the $Ag3d_{5/2}$ photoelectron peak was 1 eV. The energy scale was corrected for electrostatic charging using the Ti2p peak maximum at 458.8 eV for TiO_2. Spectra processing included subtraction of X-ray satellites and Shirley-type background [59]. Peak positions and areas were evaluated by a symmetrical Gaussian–Lorentzian curve fitting. Relative concentrations of the different chemical species were determined based on normalization of the peak areas to their photoionization cross-sections as calculated by Scofield [60].

Investigations of the catalysts by TPD were also accomplished using samples of preliminary tested materials for catalytic activity in CO hydrogenation as mentioned above. Sample handling for surface characterization was performed after preliminary treating successively in Ar and H_2 flow at 300 °C for a period of at least 30 min. TPD of hydrogen and CO was carried out in a SETARAM DSC-111 (France) differential scanning calorimeter flow reactor. A gas chromatograph equipped with thermal conductivity detector (TCD) monitored changes in outlet gas composition. Charge of studied catalyst was 95 mg. Adsorption of hydrogen was carried out at 100 °C for 1 h from a gas flow of 20 ml/min followed by cooling down to room temperature [49–51]. Carbon monoxide adsorption was accomplished at 200 °C from a

gas flow mixture of 10% CO in He (20 ml/min) for 1 h and cooling down to room temperature in the mixture. Desorption of hydrogen was implemented in Ar flow (20 ml/min) and that of CO in He flow (20 ml/min) from 27 up to 400 °C at a heating rate of 10 °C/min. Flow rates were measured by Matheson mass flow controller (USA) within 1% accuracy. The obtained desorption spectra are denoted as TPD-H_2 and TPD-CO.

Catalytic tests

Catalyst sample stability in the reaction with time on stream was studied in situ by diffuse-reflectance infrared spectroscopy (DRIFTS) by means of a FTIR Nicolet 6700 spectrometer (Thermo Electron Corporation, USA). A high temperature vacuum chamber (Thermo Spectra-Tech, USA) equipped with CaF_2 windows (1111–4000 cm^{-1}) mounted in diffuse-reflectance accessory Collector II (Thermo Electron Corporation, USA) was used and shown in Fig. 1. Spectra were recorded at a resolution of 4 (data spacing 1.928 cm^{-1}) and 100 scans. Measurements were performed using materials preliminary tested for catalytic activity in CO hydrogenation as mentioned in section Characterization technics and related calculations. Sample was preliminary treated by same way as before TPD studies, namely, in sequence in Ar and H_2 flow for 30 min at 300 °C. Experiments were carried out with 30 mg of studied sample in a flowing H_2 + CO mixture of 4:1 at a rate of 8 ml/min. (It is conformed to fact that at higher rates part of the sample can be blown away from the catalyst bed in the interior of the cell. Also, a slow flow ensures longer contact time with the catalyst surface). The measurements were performed at 250 °C within a period of 5 h. Heating to the desired level was conducted at a rate of 10 °C/min and kept further using a CAL 9400 Dual Display Autotune Temperature Controller (CAL Controls, UK, USA).

CO conversion rate K (%) was determined on the basis of integral intensity (II) of high-frequency wing of infrared band characteristic for gaseous carbon monoxide.

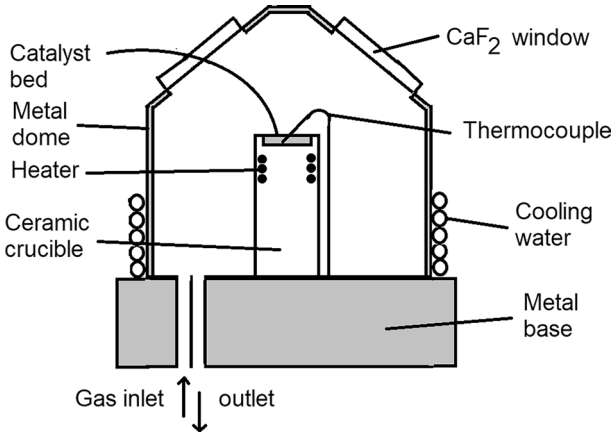

Fig. 1 Scheme of high temperature-vacuum chamber used in in situ DRIFT studies

This parameter value was calculated like a ratio between integral intensities corresponding to converted and initial CO in gas flow by the formula $K = ((II_{room} - II_i)/II_{room}).100$, where II_{room} is integral intensity of high-frequency wing of gaseous CO band determined at room temperature and II_i is integral intensity of high-frequency wing of gaseous CO band determined at 250 °C in the i-minute. As an index of the catalyst activity in the main reaction, namely $CO + 3H_2 = CH_4 + H_2O$ [50, 61–65], was used the intensity (height) of the needle-like band characteristic for CH_4.

Results and discussion

Results from characterization of studied materials

Analysis of element composition by ICP-AES showed that synthesis method used ensured very good correspondence between target and obtained quantitative characteristics about metal content (Table 1).

Dispersion determined by hydrogen chemisorption measurements showed that the specific surface of the supported metals that ensured contact with reagents was small, i.e. large metal particles were formed in the catalysts. Small surface area of applied support and operation of SMSI should not be excluded as important factors having impact on metal surface formation and could contribute in this case.

Experiments were carried out with samples of catalysts already reduced at 450 °C and tested in the reaction of CO hydrogenation [12, 13]. Table 1 reveals information about composition, metal surface, and morphology of the catalysts.

TEM and SEM together with PCCS analysis found that particles of different shape and size existed in the catalysts. Agglomerates were observed in all samples. The microscopy studies showed that common features of the studied samples were metal heterogeneous distribution in the samples and heterogeneity in particle chemical composition. A TEM image of (10%Co + 0.5%Pd)/TiO_2(red) sample reduced at 450 ºC is displayed in Fig. 2. The bright area of the image corresponded to titania support and dominant content of the metal phase was characteristic about the dark fields. A special feature of the (10%Co + 0.5%Pd)/TiO_2(red) sample was concerned with high relative part (percentage) of titanium content and absence of palladium in particle analysis. In this connection, EDX analysis showed presence of areas containing only cobalt. It could be accepted that there existed large metal particles covered by a modified titania layer of significant thickness as result from SMSI. Missing data about the presence of palladium particles can be explained by the following mechanism of reduction. Palladium was easily reduced below 100 °C before starting reduction of cobalt oxide phases (cobalt ions). The palladium particles formed were a source of nascent hydrogen participating in reduction of cobalt phases and simultaneously they could play a role of nuclei to form bimetallic particles. The surface layer of such bimetallic particles was enriched in cobalt due to migration of the cobalt atoms or agglomeration of small clusters. Observations during SEM–EDX showed that clearly outlined edges and walls of irregular geometric shapes characterized particle morphology. Agglomerates of smaller or larger size were present

Table 1 Data from different characterization techniques about composition, metal surface and morphology of catalysts from the (10%Co + 0.5%Pd)/TiO_2 system

Method, parameter (unit)	Pretreatment					
	(inert)		(ox)		(red)	
ICP-AES, element amount (wt%)	Co—9.56 Pd—0.54					
H_2 chemisorption, D_H (%)	0.8		1.2		0.8	
XPS, element concentration at the surface (atom%)	O—62.12 Ti—29.51 Co—7.90 Pd—0.47		O—62.26 Ti—29.83 Co—7.50 Pd—0.41		O—64.27 Ti—28.44 Co—6.90 Pd—0.40	
SEM–EDX, element amount (wt%)	O—53.8 Ti—42.4 Co—3.8 Pd—0.0		O—41.1 Ti—49.4 Co—9.5 Pd—0.0		O—51.0 Ti—40.7 Co—7.7 Pd—0.6	
PCCS, particle size distribution—quota (%) and particle hydrodynamic radii (nm)	90	200–430	90	200–400	100	40–120
	5	450–600	3	400–550		
	5	5000–10000	7	5000–10000		

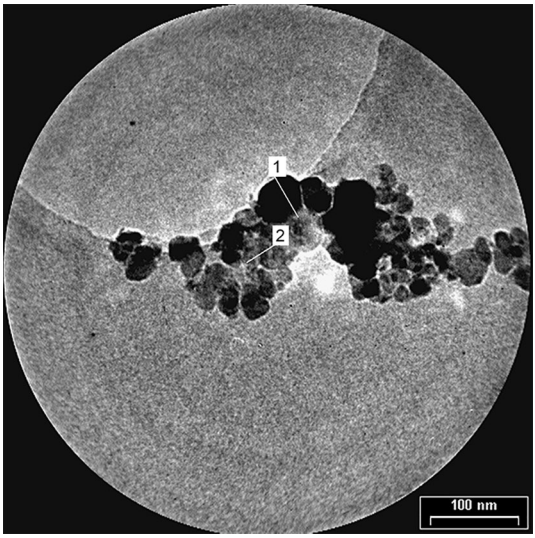

Fig. 2 TEM image of (10%Co + 0.5%Pd)/TiO_2(red) sample after reduction at 450 °C. EDX analysis: area 1: Ti-81%, Co-19%; area 2: Ti-78%, Co-22%

in the studied samples. Most formations had a clearly pronounced layered structure. It could be attributed to the used method of synthesis and fact that already formed catalysts were studied. The catalysts have worked in reaction conditions at different temperatures and phenomenon of agglomeration has reflected on the particle structure. Figs. 3 and S1 illustrate findings as layered structure and heterogeneous element distribution, respectively. PCCS revealed that all particles of

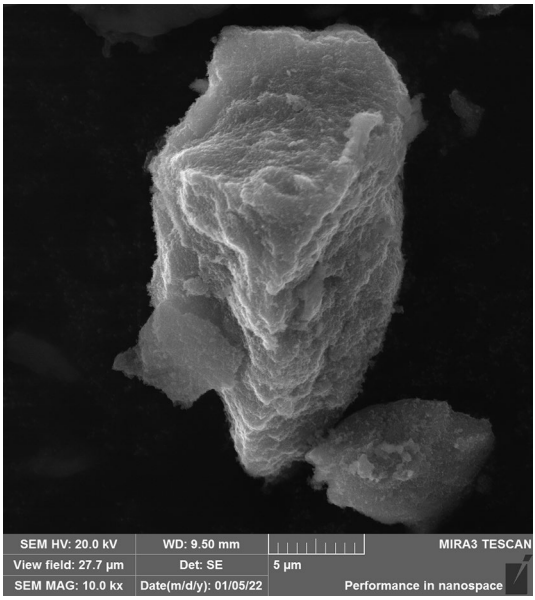

Fig. 3 SEM image of (10%Co + 0.5%Pd)/TiO_2(ox) catalyst

the (red) type of sample were of size 40–120-nm while (ox) and (inert) type catalysts exposed wider particle size distribution where larger particles predominated (Table 1).

Existence of large metal particles as chemisorption data showed and registration of agglomerates found by microscopy and PCCS investigations could be explained by the fact that all samples were reduced at 450 °C and tested under reaction conditions. Despite poor dispersion, we consider that thus prepared samples were already formed as stable catalysts and would not change during further examination or slightly changed to a little extent.

EPR measurements were carried out at a temperature of − 150 °C. All tested samples showed a broadened line to such an extent that was almost impossible to register a spectrum. Most likely this feature was due to antiferromagnetic state. However, with the (ox) catalyst, a weak signal with g-factor of 1.9751 was recorded. It was attributed to Ti^{3+} [66].

XPS study of the samples registered cobalt and palladium ions as well as metallic Pd on the surface. The presence of metals in oxidized state in the used samples was due presumably to the ex situ measurements. During exposition to air, oxygen adsorption and oxidation of the metal particle top surface layer might proceed [67, 68]. At first sight, the O/Ti ratio for the samples was 2.1–2.3, being higher than the stoichiometry for pure support (Table 1). Deconvolution of the O1s spectra (Figs. 4 and S2) showed that the latter were composed by three sub peaks [69]: (i) O in Me-O metal oxides (6–8 atom% bearing in mind stoichiometry of 1/1), (ii) O in Ti–O–Ti (40–44 atom%), (iii) O in OH groups and/or Ti^{3+} (oxygen vacancies) (8–10 atom%, 14–17 wt%). The obtained data indicated that actually the O/Ti ratio was less than 2, i.e. it was below the stoichiometric one and presuppose oxygen deficit in titania TiO_{2-x}.

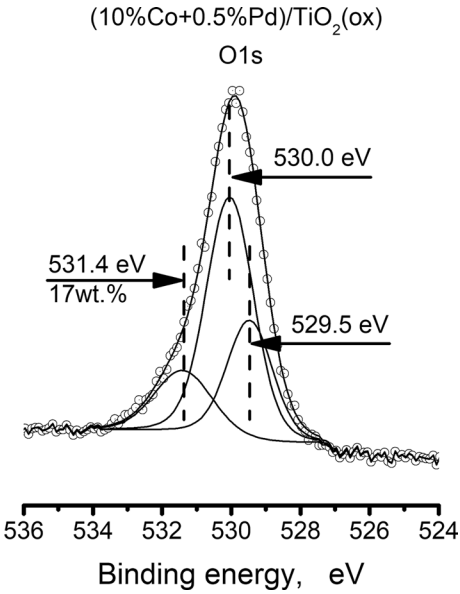

Fig. 4 High resolution O1s spectrum of (10%Co + 0.5%Pd)/TiO_2 catalyst prepared by treatment of precursor in air

Previous investigations of same systems by hydrogen chemisorption showed appearance of SMSI effect at reduction temperatures around and above 400 °C [12]. This phenomenon is not an obstacle these materials to be active catalysts for CO hydrogenation. In situ DRIFTS studies carried out at different reaction temperatures showed uncover of new metal surface at T > 150 °C [13], which is related to the produced in the process water. It has been found that effect of SMSI can be diminished by presence of water molecules [70]. Thus, EPR and XPS data showed that effect of SMSI is not totally removed. EPR and XPS results indicated availability of oxygen vacancies and Ti^{3+} ions in the catalyst(s) testifying about strong metal-support interaction (SMSI) induced during sample reduction and preserved after catalytic runs and sample exposition to air for further studies. SMSI existed in all samples, but it appeared to a highest extent in the (ox) catalyst samples (Fig. 4) where, in contrast to (red) and (inert) samples (Fig. S2), Ti^{3+} ions were detected together with the fact that the (ox) samples contained the highest oxygen-deficient titania (17%) among the three types of preliminary treated preparations.

Performance in CO hydrogenation, sites and species

Applying in situ DRIFTS, stability with time on stream (TOS) in the reaction of CO hydrogenation was followed for 5 h at 250 °C after preliminary cleaning of the sample surface at 300 °C as pointed out in the Experimental (Figs. 5 and S3). A reaction temperature of 250 °C was chosen taking into account previous experiments concerned with the effect of reaction temperature and necessity of well pronounced characteristic spectral band of CH_4 [13].

Analysis of the different spectra showed changes of band intensity with time. Increased intensity of the band at around 2143 cm^{-1} due to gaseous CO (decrease of CO conversion, respectively) and diminished intensity of the band at

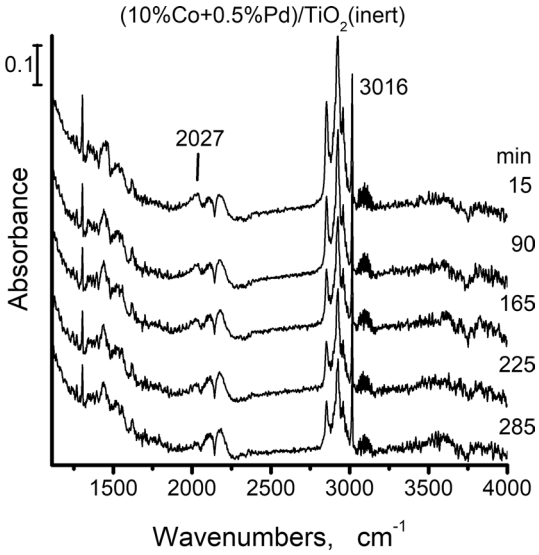

Fig. 5 In situ DRIFT spectra collected during CO hydrogenation stability tests over titania-supported cobalt–palladium catalyst prepared by treatment of precursor in Ar/N_2

3015/18 cm^{-1} characteristic of methane were observed. Band intensity diminution was also found at 2027 (Fig. 5) and 2036 cm^{-1} attributed to CO–Co^0 linear surface species (Fig. S3, B) and at 2040 cm^{-1} for CO–$Co^{\delta+}$ surface species (Fig. S3, A) [71]. Bands characteristic of linearly adsorbed CO on metallic cobalt (CO–Co^0, CO–$Co^{\delta+}$) differed in position owing to cobalt cluster size upon building up the particle. Larger clusters gave rise to bands at lower wavenumbers (2027 cm^{-1}) whereas smaller entities caused a slight blue shift (2036 cm^{-1}) [72]. Some special features should be outlined. A faster decrease in CO conversion from 50 to 35% with (inert) sample and a noticeable higher level of CO_2 formation especially with (ox) sample, as indicated by well resolved band despite its low intensity, were found. Further IR data show an insignificant decrease in intensity of the band at 2040 cm^{-1} assigned to CO–$Co^{\delta+}$ species on (ox) sample compared to the respective band in the spectra of samples of different precursor treatment. High intensity of the bands at 2958 cm^{-1} and at 2854 and 2926 cm^{-1} due to CH_3 and CH_2 groups of hydrocarbon species, respectively, [71] were also detected. Upon use of (inert) sample, the latter decreased faster with time on stream relative to the other counterparts. It seemed that CH_2 species was hardly involved in chain formation of long entities but rather occupied active surface sites. However, part of these sites did not promote smooth CH_2 species transformation [27] into methane or chain formation to higher hydrocarbons. In the opposite situation, a decrease in CH_4 formation would not have been so pronounced. This process caused some type of poisoning or blockage of the metal particle surface [17]. Bands at 2027 and 2036 cm^{-1} were broad that showed existence of different cobalt sites (with close energy) including $Co^{\delta+}$, i.e. the catalysts operated on the basis of $Co^0/Co^{\delta+}$ pair activity. The maxima showing predominant on the surface cobalt site gave also indirect information about the amount of $Co^{\delta+}$ centers. Thus at the base of 2027 cm^{-1} band could be concluded that $Co^0/Co^{\delta+}$ ratio is the largest, respectively, the $Co^{\delta+}$ was the least in the (inert) sample. Larger cobalt particles place high active surface for dissociation and hydrogenation. Probably partly positive cobalt was responsible for cleaning, dissociating and hydrogenating surface undertaking CH_3 and CH_2 species participating in their motion on the surface of catalyst. Since for the (inert)-type of sample this kind of cobalt sites was small the CH_x intermediates accumulated on the surface and deactivated catalyst in some extent.

As mentioned above the intensity of bands at 2027–2040 cm^{-1} decreased with time on stream. The samples could be arranged in descending order as (inert) > (red) ≈ (ox). Regarding initial band intensity, a different sample arrangement was formed:—(ox) > (inert) ≈ (red). The latter behavior was attributable to differences in structure and number of CO adsorption sites, and site reactivity and work on the catalyst material surface. In the case of $Co^{\delta+}$ site (band at 2040 cm^{-1}) this feature was due to reduction of cobalt, metal particle agglomeration, and cobalt segregation on the metal particle surface. Considering a Co^0 site (band at 2027 or 2036 cm^{-1}) it could be the result of metal surface decoration by partly reduced titanium oxide, i.e. a strong metal-support interaction. In addition, accumulation of hydrocarbon intermediates could be the reason with (inert)-type catalyst.

On the surface of (inert) and (red) type of the studied catalysts formation of monodentate (1358/90, 1427–45, 1534 cm^{-1}), bidentate carbonate (1267, 1534,

1622 cm^{-1}), and formate species (1358/90, 1427–45, 1534, 1622 cm^{-1}) [71] was found. In the spectra of the (inert) sample, a higher absorption at 1600 cm^{-1} was recorded as a whole. Multidirectional changes of separate bands were registered for this sample: the bands at 1427–45 and 1622 cm^{-1} increased in intensity with time on stream while the bands at 1534 and 1267 cm^{-1} remained unchanged. Comparative analysis of the variation of the intensity of individual bands in view of their association with certain surface intermediates allowed confirming an increased amount of formate species and a relatively constant quantity of bidentate carbonates on (inert) sample. It is known that during CO hydrogenation a side reaction of WGS can produce CO_2 as well that CO_2 can be obtained by CO reaction with adsorbed O species. Carbonate species are adsorption forms of carbon dioxide. Thus, the observed tendency was suggestive about a reaction mechanism regarding CO_2 release in gas phase by decomposition of bidentate carbonates on the carrier surface as registered during the experiment. In the case of (red) type of catalyst, examination of the IR band changes showed that monodentate carbonate species was predominantly formed.

Spectra of (10%Co + 0.5%Pd)/TiO_2(ox) catalyst showed formation of monodentate carbonate and formate species as illustrated by the bands at 1307/56, 1441, 1526/47 cm^{-1} and at 1356/94, 1441, 1526/47 cm^{-1}, respectively [71]. These bands increased in intensity during the experiment. It is known that CO–$Co^{\delta+}$ species is low active or inactive in CO dissociation and hydrogenation [73–75]. The observed increase in intensity of the 2040 cm^{-1} band could be due to participation of the $Co^{\delta+}$ intermediate species in CO_2 formation. An intensity increase of the bands of carbonate-(like) species could proceed because $Co^{\delta+}$ sites working as a reaction site forms CO_2 through reaction of CO–$Co^{\delta+}$ with adjacent adsorbed O species, but as an adsorption site, it was relatively strong and made difficult the transfer of carbonate intermediates to the carrier [76].

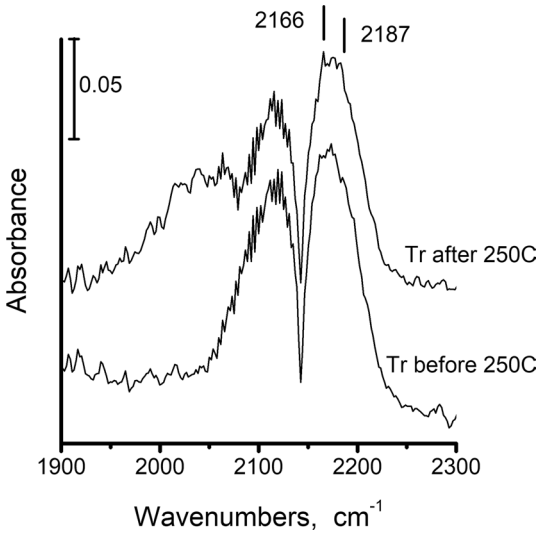

Fig. 6 DRIFT spectra of (10%Co + 0.5%Pd)/TiO_2(inert) catalyst recorded at room temperature before and after catalytic test carried out up to and at 250 °C

A spectrum of (10%Co + 0.5%Pd)/TiO_2(inert) catalyst recorded at room temperature after catalytic test (Fig. 6) manifested a slightly increased intensity of the bands at 2166 and 2187 cm^{-1}. This result gives information about employed titania support, namely about its heterogeneity. These bands were due to CO adsorption on Lewis adsorption sites of different strength and structure [39, 40, 77]. The band at 2166 cm^{-1} is characteristic of CO adsorption on five-coordinated Ti^{4+} ion bonded with two-coordinated O^{2-} ions while that at 2187 cm^{-1} is characteristic of CO adsorption on five-coordinated Ti^{4+} ion bonded to triply coordinated O^{2-} ions. This result conforms with changes of the titania support during reaction, namely, increase in surface heterogeneity.

CO conversion changed with reaction time. Integral intensity changes in time for the high-frequency wing of the gaseous CO band around 2177 cm^{-1} were used to calculate conversion. Catalytic activity was evaluated from intensity changes of the band characteristic of CH_4 product at 3015/16 cm^{-1}. Used method for calculation produces data characterized by high approximation but in the same time the data obtained show a trend of pretreatment influence on both calculated parameters. Two presumptions are accepted about same optical path in the sample and operation of surface catalyst layer only. The optical path length is connected with catalyst color, which is connected to cobalt reducibility. The samples used in the present experiment were already formed catalysts that have been consecutively reduced at 300, 400 and 450 °C and worked in CO hydrogenation. This allows to be accepted a close extent of metal reduction, same sample color (black), and close particle dispersion, i.e. close values of the optical pathway. The construction of cell for in situ studies is shown in Fig. 1. It determines such a gas flow motion that the gas is exclusively and first of all in contact with sample surface. Probably some part of the gas flow penetrates into the catalyst bed but its quota in the signal could be ignored since the catalyst bed depth is little around 2 mm compared with the surface of ~ 20 mm^2, which produces bigger part of the registered signal. Thus during the tests mainly the activity of the catalyst surface layer is registered. So, preliminary precursor treatment had a small effect on CO conversion, which slightly changed with time (Figs. 7 and S4). However, the amount of produced methane in outlet gas flow depended on pretreatment (Figs. 7 and S4) and decreased with reaction progress. A decrease by about 30% with (red) and (ox) catalyst samples was found, which reached 42% with (inert) sample.

Adsorption behavior of studied materials toward reagents H_2 and CO

In previous studies, it was established that cobalt–palladium catalyst activity depended on reduction temperature in line with changes in hydrogen adsorption [14]. In this connection comparison between the catalytic properties and hydrogen adsorption capacity after reduction at 450 °C was done. Calculations showed a a_{mono} value of 3.3 mmol/g-at_{Me} for (red) and (inert) samples and 6 mmol/g-at_{Me} for (ox)-sample. Inverse activity dependencies were found taking into account precursor-preprocessing environment. To clear up the reasons determining catalyst behavior further studies were carried out including TPD of hydrogen adsorbed at 100 °C, TPD of CO adsorbed at 200 °C, fitting of CO and hydrogen adsorption isotherms to

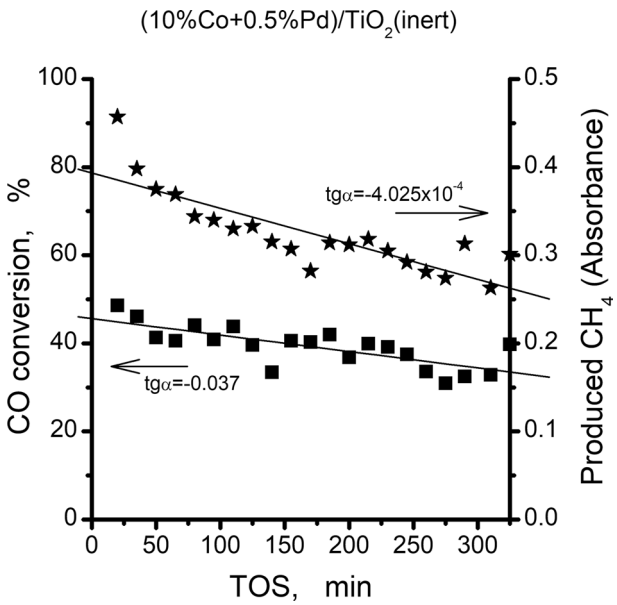

Fig. 7 CO conversion and CH_4 formation with time on stream during CO hydrogenation stability test over titania-supported cobalt–palladium catalyst prepared by treatment of precursor in Ar/N_2

the Freundlich and Langmuir models, and careful analysis of the recorded infrared spectra.

In TPD experiments adsorption of CO was performed at 200 °C. This temperature was chosen based on the catalytic tests carried out at increasing reaction temperature [13] with a view to be registered most of the adsorption forms existing on the surface of the catalysts and to be the closest one to the reaction temperature used in the time on stream examinations. TPD profiles of (10%Co + 0.5%Pd)/TiO_2 samples were characterized by specific behavior depending on pretreatment type (Fig. 8). In the case of (10%Co + 0.5%Pd)/TiO_2(red) catalyst, the main part of hydrogen was desorbed at low temperatures accompanied by a very low amount between 130 and 290 °C (Fig. 8, a, (red)). The amount of the low-temperature CO species demonstrated by the wide peak at 75 °C was larger than that of the high-temperature peaks in the interval of 200–250 °C (Fig. 8, b, (red)). High-temperature desorption species were a significant part of the adsorbed CO. In previous investigations these catalysts as well other Co–Pd samples with alumina and silica supports were tested in reaction of CO hydrogenation in conditions of increasing reaction temperature and the processes on the surface were monitored and registered in situ by DRIFTS [9, 13, 15]. Based on these in situ DRIFTS findings both the low-temperature species correspond to linear and bridged CO species whereas the high-temperature entities originated from decomposition of carbonate-(like) intermediates. It should be noted that in time on stream experiment the linearly bonded CO species was predominant.

TPD-H_2 profile with (10%Co + 0.5%Pd)/TiO_2(ox) catalyst revealed availability of three types of adsorption and desorption species. Two high-temperature desorption

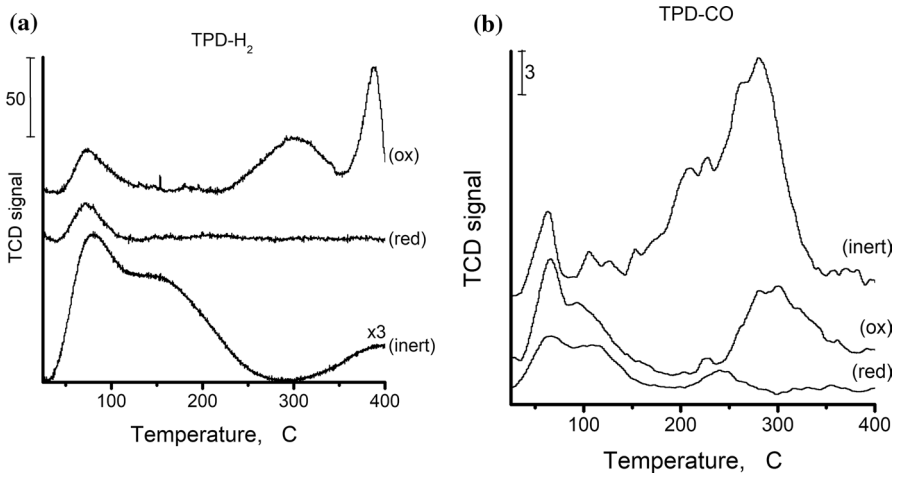

Fig. 8 TPD of H_2 adsorbed at 100 °C **(a)** and of CO adsorbed at 200 °C **(b)** on (10%Co + 0.5%Pd)/TiO_2 catalysts prepared by treatment of precursor in Ar/N_2 (inert), air (ox) and H_2 (red)

peaks with T_{max} at 300 and 400 °C dominated in the profile by 76% of the total amount of desorbed species. Desorption at 75 °C was related to low-energy adsorption sites of 23% (Fig. 8, a, (ox)). CO desorption took place within 2 ranges—below and above 200 °C—of approximately equal quantity. A narrow TPD-CO peak at 65 °C with well-pronounced shoulder around 100 °C testified desorption of almost only linearly adsorbed molecules (Fig. 8, b, (ox)). A single desorption peak at T_{max} of 275–300 °C was registered in the high-temperature range (T > 200 °C), which was due most probably to decomposition of carbonate-like intermediates.

During hydrogen desorption a (10%Co + 0.5%Pd)/TiO_2(inert) sample showed a peak of high intensity up to 200/250 °C with T_{max} around 100 °C and a shoulder at 165 °C. Weak process around 400 °C was also observed (Fig. 8, a, (inert)). The TPD-CO profile clearly manifested a much higher desorption capacity in the high-temperature region than at lower temperatures (Fig. 8, b, (inert)). The desorption process of CO occurred with maximum intensity at around 280 °C with a shoulder at around 220 °C. Desorption registered at 65 °C was assigned to linearly adsorbed CO species. Results showed that CO adsorption at 200 °C proceeded under conditions, which were optimal to form carbonate species on the surface.

Freundlich isotherm exponent 1/n derived on the basis of hydrogen chemisorption had similar values for (ox) and (inert) samples (Table 2) and a highest value for (10%Co + 0.5%Pd)/TiO_2(red) catalyst. Thus, the exponent 1/n distinguished the (red) catalyst as having the highest extent of surface homogeneity amongst the three types of samples. TPD-H_2 data showed definitely the presence of both low-temperature and high-temperature species of adsorbed hydrogen. Again, the (10%Co + 0.5%Pd)/TiO_2(red) catalyst was an exception characterized by complete desorption bellow 250 °C. A general conclusion could be made about the high-temperature desorption that the process was intense around 300 °C from (ox) sample and at $T_{max} \geq 380$ °C with both (ox) and (inert) samples (Fig. 8, a). Thus, it could be

Table 2 Calculated data about hydrogen chemisorption at 100 °C and irreversible CO chemisorption at room temperature on (10%Co + 0.5%Pd)/TiO_2 catalysts reduced at 450 °C: 1/n—exponent in Freundlich model; K_L—Langmuir constant ($Torr^{-1}$); R^2—coefficient of determination

Gas	Parameter	Pretreatment		
		(inert)	(ox)	(red)
H_2	1/n (R^2)	0.1913 (0.9889)	0.1718 (0.9516)	0.2500 (0.9984)
	K_L (R^2)	0.1296 (0.9924)	0.1270 (0.9819)	0.1019 (0.9906)
CO	1/n (R^2)	0.1098 (0.9809)	0.1177 (0.9805)	0.4253 (0.6985)
	K_L (R^2)	0.2235 (0.9959)	0.1881 (0.9955)	0.0668 (0.9955)

affirmed that heterogeneity was not only similar relative to 1/n values but also it was of the same kind as based on adsorption site type.

The trend about the pretreatment influence on the exponent 1/n values for hydrogen adsorption was valid also for CO adsorption. According to data listed in Table 2 the (red) sample was the most homogeneous in relation to CO adsorption. The other two samples had 1/n parameters of almost the same value determining similarity in this their property. Two regions, low- and high-temperature, were well distinguished in TPD-CO patterns of (inert) and (ox) samples (Fig. 8, b). Parallel analysis of heterogeneity in relation to both reagents found that the exponent values showed relatively higher homogeneity of (red) sample surface for CO adsorption in comparison to that toward hydrogen. In case of the other two catalysts ((inert) and (ox) type) was observed the opposite behavior, i.e. homogeneity related to hydrogen chemisorption was higher than that toward CO.

Langmuir constant K_LH_2 values about hydrogen as adsorbate were calculated based on experimental data fitting to Langmuir model of adsorption (Table 2). Considering pretreatment type comparison between K_L values and the amount of CO hydrogenation product, namely methane, showed a concurrence in K_L changes, ΔH_{ads} change being opposite, and CH_4 amount (Figs. 5 and S3). Sample K_LH_2 values were of the same order and one more time the (red)-type samples were characterized amongst all by higher enthalpy of adsorption (Table 2). This indicated that E_{ads} ($\Delta H_{ads} = E_{ads} - E_{des}$) was relatively high, which determined more difficult adsorption and, therefore, adsorbate amount was small. As a whole, a smaller adsorbate amount and lower E_{des} values resulted in an easy desorption from (red)-type samples. Desorption from the other two types of samples was somewhat more difficult as it was evident from the TPD study at higher temperatures.

Regarding CO adsorption the observations about Langmuir constant for hydrogen chemisorption was in force as a whole but the valid inequality is (inert) > (ox) >> (red). K_LCO value was quite lower in case of (red) type of catalyst (Table 2). Comparison of K_L values for the two reagents showed that $K_LCO < K_LH_2$ relation was valid in case of (red/ox) samples. However, the inequality had opposite sign (reverse order) in case of (inert) sample $K_LCO > K_LH_2$, respectively $\Delta H_{ads}CO < \Delta H_{ads}H_2$ and $(E_{ads} - E_{des})CO < (E_{ads} - E_{des})H_2$. This was indicative about lower activation energy of CO adsorption and higher activation energy of CO desorption, which supposed large amount of adsorbate on the surface.

Conversely adsorption of hydrogen was characterized by increased activation energy and decreased activation energy of desorption that surmised smaller amount of adsorbate on the surface. The (inert)-type of catalyst had high initial activity in CO hydrogenation. It seems in such a case of easy hydrogenation the amounts of hydrogen available on the surface were not enough hydrogenation to be completed. Thus products of incomplete hydrogenation of CH_x intermediates contributed to the decrease in sample activity.

It is worth noticing the very good coincidence of conclusions based on adsorption isotherm calculations and desorption experiments in relation to hydrogen adsorption and available sites as illustrated by TPD-H_2 data and isotherm parameters. First, the (red)-sample surface exposed active sites of highest homogeneity and, second, the surface of (ox) and (inert) samples revealed a higher site heterogeneity. Despite CO chemisorption was carried out at room temperature the found trends were useful in clearing up some details.

Heterogeneity of sites and relation toward adsorption and/or reaction activity

The behavior of the infrared bands at 2027–2040 cm^{-1} assigned to atop adsorption of carbon monoxide and the TPD-CO peaks below 100 °C in the low-temperature region were compared. On attaining reaction equilibrium in the course of IR measurements, the band intensities decreased in the order (inert) > (red) > (ox) (Figs. 7 and S4). Bearing in mind intensity the peaks with T_{max} of desorption at 63/66 °C arranged in the order (red) < (inert) < (ox). Thus, a conclusion was derived that adsorption sites on (ox) type of catalyst for the formation of atop CO species were of relatively high strength whereas (inert) sample surface exposed weak sites for the same species. In view of the high intensity bands for methane, during reaction the adsorption sites have converted into very active reaction centers. The decrease in intensity of the CH_4 band and the registered CO_2 bands allowed supposition that a certain part of the CO hydrogenation reaction sites might have exhibited some activity for water–gas shift reaction. It is known that contact time is a crucial factor for determining the formation of CO_2 and hydrocarbons as the latter needs longer residence time on the catalyst surface [78].

Analysis of TPD-CO data, especially TCD signal intensity around 250 °C, and in situ DRIFTS records below 1600 cm^{-1} during catalytic stability examinations showed adsorption sites of medium and high strength as well as highly or moderately stable intermediates on (10%Co + 0.5%Pd)/TiO_2(red) samples. In this connection (10%Co + 0.5%Pd)/TiO_2(ox) samples exposed adsorption sites of high strength and highly stable carbonate-like species was detected. However, adsorption sites of variable strength and intermediates of various stability on (10%Co + 0.5%Pd)/TiO_2(inert) samples were found but sites of medium to high strength and highly and moderately stable intermediates were predominant.

For all samples, observed changes in the infrared region below 1600 cm^{-1} and desorption intensity around 250 °C in the TPD profiles suggested that on the surface of the (10%Co + 0.5%Pd)/TiO_2 catalytic system a significant amount of

weakly bonded carbonate species was formed at 250 °C. Most probably, bidentate species was present that easily decomposed to form carbon dioxide [41].

Experimental data obtained with (inert) samples allowed further conclusions concerned with adsorption and reaction site heterogeneity. Taking into account presumption that hydrogen and CO adsorb on the same sites of reduced metal atoms the obtained data generally showed that active sites were of relatively weak to medium strength in relation to hydrogen adsorption but in terms of CO adsorption most sites were relatively strong. It was mentioned above that sites of medium to high strength and moderately and highly stable species were predominant. Due to sample behavior during in situ activity studies, availability of bidentate carbonates could be associated with medium-strength reaction sites. Monodentate carbonates and formate species were assigned to availability of strong sites on the surface. Hence, weak sites in relation to CO adsorption most probably played a role of active sites in the reaction of hydrogenation as stated above. Infrared spectra proved easy hydrogenation by high intensity bands at 2854, 2926, and 2958 cm^{-1} characteristic of CH_x groups. In view of the results about methane formation, namely a decrease with time on stream by 42%, it could be concluded that the reaction sites for CO hydrogenation were of high strength in terms of adsorption of CH_x species.

Conclusions

Results of H_2 chemisorption on (10%Co + 0.5%Pd)/TiO_2 catalysts reduced successively at 300 and 400 °C for 1 h and at 450 °C for 2 h showed that the metal particles' surface heterogeneity was similar and of the same type, i.e. the same type of sites of similar strength for adsorbate bonding were exposed independently of the preliminary treatment procedure in oxidative, reduction or inert gas media applied to catalyst precursor prepared by impregnation.

Regarding CO chemisorption, adsorption site strength and stability of the intermediates depended on the preliminary treatment of the catalyst precursor. Generally, sites of medium and high strength and stability were predominant in all samples. The highest diversity in site strength and stability of intermediates on the surface demonstrated (10%Co + 0.5%Pd)/TiO_2(inert) catalyst.

Use of in situ FTIRS and carbon monoxide as probe molecule due to its sensitivity in adsorption on various sites allowed registration of site heterogeneity on the surface of titania support, too. In addition, a more precise analysis of chemisorption, TPD, and infrared data could help in differentiation of adsorption sites by strength and structure so as activity of reaction sites.

Analysis of in situ IRS data from (10%Co + 0.5%Pd)/TiO_2(inert) catalyst behavior in CO hydrogenation allowed more detailed description of adsorption and reaction site dynamics. The weak sites in relation to CO adsorption most probably played a role of active sites in the reaction of CO hydrogenation but were of high strength in terms of adsorption sites of CH_x species.

SMSI existed in all catalysts but it appeared to a highest extent in catalyst obtained from precursor treated in oxidative media due to formed higher metal particle dispersion.

Supplementary Information The online version contains supplementary material available at https://doi.org/10.1007/s11144-024-02644-8.

Acknowledgements This work was supported by Bulgarian Academy of Sciences under Grant IC-SK/02/2023-2024 and Slovak Academy of Sciences through Grant BAS-SAS-2022-06. Research equipment of distributed research infrastructure INFRAMAT (part of Bulgarian national roadmap for research infrastructures) supported by Bulgarian Ministry of Education and Science was used in this investigation. M. Fabian thanks Slovak Research and Development Agency APVV (Contract No. 19-0526). H. Kolev thanks Bulgarian National Science Fund (Contract No. KP-06-Dunav/4).

Author contributions Conceptualization, writing—original draft preparation, visualization, project administration, funding acquisition [Maya Shopska]; methodology [Maya Shopska, Georgi Kadinov]; validation [Maya Shopska, Krassimir Tenchev, Martin Fabian, Hristo Kolev, Katerina Aleksieva]; investigation [Maya Shopska, Krassimir Tenchev, Hristo Kolev, Martin Fabian, Katerina Aleksieva, Georgi Kadinov]; resources [Maya Shopska, Martin Fabian]; data curation [Maya Shopska, Krassimir Tenchev, Hristo Kolev, Martin Fabian, Katerina Aleksieva, Georgi Kadinov]; writing—review and editing [Georgi Kadinov]; supervision [Georgi Kadinov].

Funding The research leading to these results received funding from Bulgarian and Slovak Academies of Sciences, by contracts IC-SK/02/2023–2024 and BAS-SAS-2022-06.

Data availability All datasets for this study are included in the manuscript. They also are available in IC, BAS, Sofia, Bulgaria; IG, SAS, Kosice, Slovakia.

Code availability Not applicable.

Declarations

Competing interests The authors have no conflicts of interest to declare that are relevant to the content of this article.

Ethical approval Ethics approval was not required for this research.

Consent for publication All authors have read and agreed to the published version of the manuscript.

References

1. Dry ME (2002) The Fischer–Tropsch process: 1950–2000. Catal Today 71:227–241. https://doi.org/10.1016/S0920-5861(01)00453-9
2. Mahmoudi H, Mahmoudi M, Doustdar O, Jahangiri H, Tsolakis A, Gu S, LechWyszynski M (2017) A review of Fischer–Tropsch synthesis process, mechanism, surface chemistry and catalyst formulation. Biofuels Eng 2:11–31. https://doi.org/10.1515/bfuel-2017-0002
3. Rabo JA, Risch AP, Poutsma ML (1978) Reactions of carbon monoxide and hydrogen on Co, Ni, Ru, and Pd metals. J Catal 53:295–311. https://doi.org/10.1016/0021-9517(78)90102-1
4. Davis BH, Iglesia E (2002) Technology development for iron and cobalt Fischer–Tropsch catalysts, Final technical report DE-FC26-98FT40308. University of California at Berkeley & University of Kentucky Research Foundation
5. Arsalanfar M, Mirzaei AA, Bozorgzadeh HR, Samimi A (2014) A review of Fischer–Tropsch synthesis on the cobalt based catalysts. Phys Chem Res 2:179–201. https://doi.org/10.22036/PCR.2014.5786
6. Mallat T, Szabo S, Petro J, Mendioroz S, Folgado MA (1989) Real and apparent dispersion of carbon supported palladium-cobalt catalysts. Appl Catal 53:29–40. https://doi.org/10.1016/S0166-9834(00)80007-X

7. Noronha FB, Schmal M, Moraweck B, Delichere P, Brun M, Villain F, Frety R (2000) Characterization of niobia-supported palladium-cobalt catalysts. J Phys Chem B 104:5478–5485. https://doi.org/10.1021/jp992777o
8. Sun S, Fujimoto K, Yoneyama Y, Tsubaki N (2002) Fischer–Tropsch synthesis using Co/SiO_2 catalysts prepared from mixed precursors and addition effect of noble metals. Fuel 81:1583–1591. https://doi.org/10.1016/S0016-2361(02)00090-X
9. Shopska M, Kolev H, Aleksieva K, Shtereva I, Tenchev K, Todorova S, Fabian M, Kadinov G (2021) Study of sites and species during CO hydrogenation over SiO_2-supported Co–Pd catalysts. Relation to performance in the process. Reac Kinet Mech Catal 134:303–330. https://doi.org/10.1007/s11144-021-02067-9
10. Lapidus AL, Krylova AYu, Kozlova GV, Kondratiev LT, Myshenkova TN, Babenkova LV, Kulievskaya YuG, Sominskii SD (1990) Synthesis of hydrocarbons from CO and H_2 in presence of supported Co catalysts modified with palladium. Russ Chem Bull 39:521–524
11. Lapidus AL, Krylova AYu, Tonkonogov VP, Izzuka DOCh, Kapoor MP (1995) Influence of palladium addition on properties of Co catalysts in synthesis of hydrocarbons from CO and H_2. Solid Fuel Chem 3:90–92
12. Shopska M, Kadinov G (2009) Catalytic performance of 10%Co+0.5%Pd/TiO_2 systems obtained by treatment in different gaseous media. Bulg Chem Ind 80:34–38
13. Shopska MG, Shtereva IZh, Kolev HG, Aleksieva KI, Todorova SZh, Kadinov GB (2020) Activity and selectivity of Co–Pd/TiO_2 catalysts in CO hydrogenation. Bulg Chem Commun 52:320–327. https://doi.org/10.34049/bcc.52.2.BCS7
14. Shopska MG, Kadinov GB (2010) Influence of the support on the physico-chemical properties of bimetallic Co–Pd catalysts prepared by pretreatment in an inert atmosphere. Asian Chem Lett 14:111–118
15. Shopska MG, Shtereva IZ, Kolev HG, Tenchev KK, Todorova SZ, Kadinov GB (2020) Role of the various surface sites and species in CO hydrogenation over alumina-supported Co–Pd catalysts. Croat Chem Acta 93(2):121–131. https://doi.org/10.5562/cca3649
16. Paredes-Nunez A, Jbir I, Bianchi D, Meunier FC (2015) Spectrum baseline artefacts and correction of gas-phase species signal during diffuse reflectance FT-IR analyses of catalysts at variable temperatures. Appl Catal A: Gen 495:17–22. https://doi.org/10.1016/j.apcata.2015.01.042
17. Paredes-Nunez A, Lorito D, Guilhaume N, Mirodatos C, Schuurman Y, Meunier FC (2015) Nature and reactivity of the surface species observed over a supported cobalt catalyst under CO/H_2 mixtures. Cat Tod 242:178–183. https://doi.org/10.1016/j.cattod.2014.04.033
18. Jeroro E, Hyman MP, Vohs JM (2009) Ensemble vs. electronic effects on the reactivity of two-dimensional Pd alloys: a comparison of CO and CH_3OH adsorption on Zn/Pd(111) and Cu/Pd(111). Phys Chem Chem Phys 11:10457–10465. https://doi.org/10.1039/B913220A
19. Scalbert J, Clémençon I, Lecour P, Braconnier L, Diehl F, Legens C (2015) Simultaneous investigation of the structure and surface of a Co/alumina catalyst during Fischer–Tropsch synthesis: discrimination of various phenomena with beneficial or disadvantageous impact on activity. Catal Sci Technol 5:4193–4201. https://doi.org/10.1039/C5CY00556F
20. Smith ML, Kumar N, Spivey JJ (2012) CO adsorption behavior of Cu/SiO_2, Co/SiO_2, and CuCo/SiO_2 catalysts studied by in situ DRIFTS. J Phys Chem C 116:7931–7939. https://doi.org/10.1021/jp301197s
21. Khodakov AYu, Lynch J, Bazin D, Rebous B, Zanier N, Moisson B, Chaumette P (1997) Reducibility of cobalt species in silica-supported Fischer–Tropsch catalysts. J Catal 168:16–25
22. Rodrigues EL, Bueno JMC (2002) Co/SiO_2 catalysts for selective hydrogenation of crotonaldehyde II: influence of the Co surface structure on selectivity. Appl Catal A: General 232:147–158. https://doi.org/10.1016/S0926-860X(02)00090-X
23. Kumar N, Stanley GG, Spivey JJ (2019) Effect of H_2 preadsorption on CO interactions with a Co/Re/Zr/SiO_2-based catalyst: in situ DRIFTS study. J Phys Chem C 123(9):5394–5400. https://doi.org/10.1021/acs.jpcc.8b10731
24. Song D, Li J, Cai Q (2007) In situ diffuse reflectance FTIR study of CO adsorbed on a cobalt catalyst supported by silica with different pore sizes. J Phys Chem 111:18970–18979. https://doi.org/10.1021/jp0751357
25. Xie S, Choi S-I, Xia X, Xia Y (2013) Catalysis on faceted noble-metal nanocrystals: both shape and size matter. Curr Opin Chem Eng 2:142–150. https://doi.org/10.1016/j.coche.2013.02.003

26. ten Have IC, Kromwijk JJG, Monai M, Ferri D, Sterk EB, Meirer F, Weckhuysen BM (2022) Uncovering the reaction mechanism behind CoO as active phase for CO_2 hydrogenation. Nat Commun 13:324–334. https://doi.org/10.1038/s41467-022-27981-x
27. Paredes-Nunez A, Lorito D, Burel L, Motta-Meira D, Agostini G, Guilhaume N, Schuurman Y, Meunier F (2018) CO hydrogenation on cobalt-based catalysts: tin poisoning unravels CO in hollow sites as a main surface intermediate. Ang Chem Int Ed 57:547–550
28. Madon R, Taylor W (1981) Fischer–Tropsch synthesis on a precipitated iron catalyst. J Catal 69:32–43. https://doi.org/10.1016/0021-9517(81)90125-1
29. Schulz H, Van Steen E, Claeys M (1995) Specific inhibition as the kinetic principle of the Fischer–Tropsch synthesis. Top Catal 2:223–234. https://doi.org/10.1007/BF01491969
30. Zhang R, Kang L, Liu H, He L, Wang B (2018) Insight into the C–C chain growth in Fischer–Tropsch synthesis on HCP Co(10–10) surface: the effect of crystal facets on the preferred mechanism. Comput Mater Sci 145:263–279. https://doi.org/10.1016/j.commatsci.2018.01.013
31. Liu H, Zhang R, Ling L, Wang Q, Wang B, Li D (2017) Insight into the preferred formation mechanism of long-chain hydrocarbons in Fischer–Tropsch synthesis on Hcp Co(10–11) surfaces from DFT and microkinetic modeling. Catal Sci Technol 7:3758–3776. https://doi.org/10.1039/C7CY01436H
32. Savitskii EM, Polyakova VP, Gorina NB, Roshan NR (1975) Metallurgy of platinum metals. Metallurgy Publication
33. Matsuo Y (1972) Ordered alloys in the cobalt–palladium system. J Phys Soc Japan 32:972–978. https://doi.org/10.1143/JPSJ.32.972
34. Matsuo Y, Hayashi F (1970) Ordered phase in the Co–Pd system. J Phys Soc Japan 28:1375. https://doi.org/10.1143/JPSJ.28.1375
35. Noordermeer A, Kok GA, Nieuwenhuys BE (1986) Comparison between the adsorption properties of Pd(111) and PdCu(111) surfaces for carbon monoxide and hydrogen. Surf Sci 172:349–362. https://doi.org/10.1016/0039-6028(86)90760-0
36. Sakong S, Mosch C, Groß A (2007) CO adsorption on Cu–Pd alloy surfaces: ligand versus ensemble effects. Phys Chem Chem Phys 9:2216–2225. https://doi.org/10.1039/B615547B
37. Belskaya OB, Danilova IG, Kazakov MO, Mironenko RM, Lavrenov AV, Likholobov VA (2012) FTIR spectroscopy of adsorbed probe molecules for analyzing the surface properties of supported Pt(Pd) catalysts. In: Theophanides T (ed) Infrared spectroscopy—materials science, engineering and technology. InTech, Rijeka
38. Bolis V, Fubini B, Garrone E, Morterra C, Ugliengo P (1992) Induced heterogeneity at the surface of group 4 dioxides as revealed by CO adsorption at room temperature. J Chem Soc Faraday Trans 88:391–398. https://doi.org/10.1039/FT9928800391
39. Concepcion P, Reddy BM, Knoezinger H (1999) FTIR study of low—temperature CO adsorption on pure Al_2O_3–TiO_2 and V/Al_2O_3–TiO_2 catalysts. Phys Chem Chem Phys 1:3031–3037. https://doi.org/10.1039/A901776C
40. Ferretto L, Glisenti A (2003) Surface acidity and basicity of a rutile powder. Chem Mater 15:1181–1188. https://doi.org/10.1021/cm021269f
41. Szanyi J, Kwak JH (2014) Dissecting the steps of CO_2 reduction: 1. The interaction of CO and CO_2 with γ-Al_2O_3: an in situ FTIR study. Phys Chem Chem Phys 16:15117–15125. https://doi.org/10.1039/C4CP00616J
42. Anderson JR (1978) Structure of metallic catalysts. Mir, Moscow
43. Hadjiivanov KI, Klissurski DG (1996) Surface chemistry of titania (anatase) and titania-supported catalysts. Chem Soc Rev 25:61–69. https://doi.org/10.1039/CS9962500061
44. Nobile A Jr, Davis MW Jr (1989) Importance of the anatase-rutile phase transition and titania grain enlargement in the strong metal-support interaction phenomenon in $FeTiO_2$ catalysts. J Catal 116:383–398. https://doi.org/10.1016/0021-9517(89)90105-X
45. Riva R, Miessner H, Del Piero G, Rebours D, Roy M (1998) Dispersion and reducibility of Co/SiO_2 and Co/TiO_2. Stud Surf Sci Catal 119:203–208. https://doi.org/10.1016/S0167-2991(98)80432-1
46. Satterfield CN (1991) Heterogeneous catalysis in industrial practice. McGraw-Hill, New York
47. Voß M, Borgmann D, Wedler G (2002) Characterization of alumina, silica, and titania supported cobalt catalysts. J Catal 212:10–21. https://doi.org/10.1006/jcat.2002.3739
48. Shopska M, Kadinov G, Kiennemann A (2000) Influence of noble metal (Pd, Pt) and reduction mode of supported cobalt catalysts on hydrogen adsorption. Sci Rept Union Mechan Engng 54(3):132–137

49. Aben PC (1968) Palladium areas in supported catalysts: determination of palladium surface areas in supported catalysts by means of hydrogen chemisorption. J Catal 10:224–229. https://doi.org/10.1016/S0021-9517(68)80002-8
50. Reuel RC, Bartholomew CH (1984) The stoichiometries of H_2 and CO adsorptions on cobalt: effects of support and preparation. J Catal 85:63–77. https://doi.org/10.1016/0021-9517(84)90110-6
51. Zowtiak JM, Bartholomew CH (1983) The kinetics of H_2 adsorption on and desorption from cobalt and the effects of support thereon. J Catal 83:107–120. https://doi.org/10.1016/00219517(83)90034-9
52. Adamson AW (1979) Physical chemistry of surfaces. Mir, Moscow
53. Rashidi NA, Yusup S, Borhan A (2016) Isotherm and thermodynamic analysis of carbon dioxide on activated carbon. Pro Eng 148:630–637. https://doi.org/10.1016/j.proeng.2016.06.527
54. Thomas JM, Thomas WJ (1969) Introduction to the principles of heterogeneous catalysis. Mir, Moscow
55. Osmari TA, Gallon R, Schwaab M, Barbosa-Coutinho E, Severo JB Jr, Pinto JC (2013) Statistical analysis of linear and non—linear regression for the estimation of adsorption isotherm parameters. Adsorp Sci Technol 31:433–458. https://doi.org/10.1260/0263-6174.31.5.433
56. Barka N, Ouzaouit K, Abdennouri M, Makhfouk ME (2013) Dried prickly pear cactus (*Opuntia ficus* indica) cladodes as a low-cost and eco-friendly biosorbent for dyes removal from aqueous solutions. J Taiwan Inst Chem Eng 44:52–60. https://doi.org/10.1016/j.jtice.2012.09.007
57. Madaeni SS, Salehi E (2009) Adsorption of cations on nanofiltration membrane: separation mechanism, isotherm confirmation and thermodynamic analysis. Chem Eng J 150:114–121. https://doi.org/10.1016/j.cej.2008.12.005
58. Romero JRG, Moreno-Piraján JC, Gutierrez LG (2018) Kinetic and equilibrium study of the adsorption of CO_2 in ultramicropores of resorcinol—formaldehyde aerogels obtained in acidic and basic medium. Carbon 4(4):52. https://doi.org/10.3390/c4040052
59. Shirley D (1972) High-resolution X-ray photoemission spectrum of the valence bands of gold. Phys Rev B 5:4709–4714. https://doi.org/10.1103/PhysRevB.5.4709
60. Scofield JH (1976) Hartree–Slater subshell photoionization cross-sections at 1254 and 1487 eV. J Electron Spectrosc Relat Phenom 8:129–137. https://doi.org/10.1016/0368-2048(76)80015-1
61. Dwyer DJ, Yoshida K, Somorjai GA (1979) Hydrocarbon synthesis from carbon monoxide and hydrogen. American Chemical Society, Washington, DC, p 65
62. Vannice MA, Lam YL, Garten RL (1979) Hydrocarbon synthesis from carbon monoxide and hydrogen. American Chemical Society, Washington, DC, p 25
63. Moon SH, Yoon KE (1985) Kinetic behavior of partially reduced Co/Al_2O_3 catalysts in CO hydrogenation. Appl Catal 16:289–300. https://doi.org/10.1016/S0166-9834(00)84394-8
64. Lee D-K, Lee J-H, Ihm S-K (1988) Effect of carbon deposits on carbon monoxide hydrogenation over alumina-supported cobalt catalyst. Appl Catal 36:199–207. https://doi.org/10.1016/S0166-9834(00)80115-3
65. Enache DI, Rebous B, Roy-Auberger M, Revel R (2002) In situ XRD study of the influence of thermal treatment on the characteristics and the catalytic properties of cobalt-based Fischer–Tropsch catalysts. J Catal 205:346–353. https://doi.org/10.1006/jcat.2001.3462
66. Claus P, Schimpf S, Schodel R, Kraak P, Morke W, Honicke D (1997) Hydrogenation of crotanaldehyde on Pt/TiO_2 catalysts: Influence of the phase composition of titania on activity. Appl Catal A: Gen 165:429–441. https://doi.org/10.1016/S0926-860X(97)00224-X
67. Popova NM, Babenkova LV, Savel'eva GA (1979) Adsorption and interaction of simple gases with VIIIth group metals. Nauka, Alma-Ata
68. Potoczna-Petru D, Jablonski JM, Okal J, Krajczyk L (1998) Influence of oxidation-reduction treatment on microstructure of Co/SiO_2 catalysts. Appl Catal A 175:113–120. https://doi.org/10.1016/S0926-860X(98)00214-2
69. Hadjiivanov K, Vayssilov G (2002) Characterization of oxide surfaces and zeolites by carbon monoxide as an IR probe molecule. Adv Catal 47:307–511. https://doi.org/10.1016/S0360-0564(02)47008-3
70. Li J, Xu L, Keogh RA, Davis BH (2000) Effect of boron and ruthenium on the catalytic properties of Co/TiO_2 Fischer–Tropsch catalysts. ACS Div Petr Chem 45:253–255
71. Little LH (1966) Infrared spectra of adsorbed species. Academic Press Inc., London
72. Sun S, Tsubaki N, Fujimoto K (2000) The reaction performances and characterization of Fischer–Tropsch synthesis Co/SiO_2 catalysts prepared from mixed cobalt salts. Appl Catal A: Gen 202:121–131. https://doi.org/10.1016/S0926-860X(00)00455-5

73. Blyholder G (1964) Molecular orbital view of chemisorbed carbon monoxide. J Phys Chem 68:2772–2777. https://doi.org/10.1021/j100792a006
74. Kadinov G, Bonev Ch, Todorova S, Palazov A (1998) IR spectroscopy study of CO adsorption and of the interaction between CO and hydrogen on alumina supported cobalt. J Chem Soc Faraday Trans 94:3027–3031. https://doi.org/10.1039/A804315I
75. Rygh LES, Ellestad OH, Klæboe P, Nielsen CJ (2000) Infrared study of CO adsorbed on Co/γ-Al_2O_3 based Fischer–Tropsch catalysts; semi-empirical calculations as a tool for vibrational assignments. Phys Chem Chem Phys 2:1835–1846. https://doi.org/10.1039/B000188K
76. Matolinova I, Fabik S, Masek K, Sedlacek L, Skala T, Veltruska K, Matolin V (2003) Influence of Pd–Co bimetallic interaction on CO adsorption properties of Pd_xCo_{1-x} alloys: XPS, TPD and static SIMS studies. Vacuum 71:41–45. https://doi.org/10.1016/S0042-207X(02)00711-X
77. Hadjiivanov K, Lamotte J, Lavalley J-C (1997) FTIR study of low-temperature CO adsorption on pure and ammonia-precovered TiO_2 (anatase). Langmuir 13:3374–3381. https://doi.org/10.1021/la962104m
78. Sethuraman R, Bakhshi NN, Katikaneni SP, Idem RO (2001) Fischer–Tropsch synthesis in a follow bed reactor consisting of Co–Ni–ZrO_2 and sulfated-ZrO_2 catalyst beds. Fuel Proc Technol 73:197–222. https://doi.org/10.1016/S0378-3820(01)00199-0

Authors and Affiliations

Maya Shopska[1] · Krassimir Tenchev[1] · Georgi Kadinov[1] · Hristo Kolev[1] · Martin Fabian[2] · Katerina Aleksieva[1]

✉ Maya Shopska
shopska@ic.bas.bg

Krassimir Tenchev
tenchev@ic.bas.bg

Georgi Kadinov
kadinovg@ic.bas.bg

Hristo Kolev
hgkolev@ic.bas.bg

Martin Fabian
fabianm@saske.sk

Katerina Aleksieva
kati@ic.bas.bg

1 Institute of Catalysis, Bulgarian Academy of Sciences, Acad. G. Bonchev St., Bldg. 11, 1113 Sofia, Bulgaria

2 Institute of Geotechnics, Slovak Academy of Sciences, Watsonova 45, 04001 Kosice, Slovak Republic